

The periodic variations of a white–light flare observed with ULTRACAM

M. Mathioudakis¹, D.S. Bloomfield¹, D.B. Jess¹, V.S. Dhillon², and T.R. Marsh³

¹ Department of Physics and Astronomy, Queen’s University Belfast, Belfast, BT7 1NN,
Northern Ireland, UK

² Department of Physics and Astronomy, University of Sheffield, Sheffield, S3 7RH, UK

³ Department of Physics, University of Warwick, Coventry, CV4 7AL, UK

Received date / Accepted date

Abstract. High time resolution observations of a white–light flare on the active star EQ PegB show evidence of intensity variations with a period of ≈ 10 s. The period drifts to longer values during the decay phase of the flare. If the oscillation is interpreted as an impulsively–excited, standing–acoustic wave in a flare loop, the period implies a loop length of ≈ 1.7 Mm and ≈ 3.4 Mm for the case of the fundamental mode and the second harmonic, respectively. However, the small loop lengths imply a very high modulation depth making the acoustic interpretation unlikely. A more realistic interpretation may be that of a fast–MHD wave, with the modulation of the emission being due to the magnetic field. Alternatively, the variations could be due to a series of reconnection events. The periodic signature may then arise as a result of the lateral separation of individual flare loops or current sheets with oscillatory dynamics (*i.e.*, periodic reconnection).

Key words. Waves – Stars: activity – Stars: atmospheres – Stars: flare – Stars: individual:
EQ Peg

1. Introduction

The detection of oscillations in coronal loops has provided clear evidence for waves in the upper solar atmosphere (Nakariakov & Verwichte 2005). These observations provide new insights into the processes of atmospheric heating. They have also raised the prospect of using oscillations as a diagnostic to infer the properties of the upper solar atmosphere and allowed the development of coronal seismology (Roberts 2000). For example, Nakariakov & Ofman (2001) developed a method for determining an absolute value for the magnetic field strength of coronal loops that oscillate as a result of standing kink–mode waves. The crucial theory of MHD oscillations

Send offprint requests to: M. Mathioudakis, e-mail: M.Mathioudakis@qub.ac.uk

in solar atmospheric structures has been presented by Roberts, Edwin, & Benz (1984), where both standing and propagating wave modes are considered. Coronal structures, such as the loops within an active region, can act as wave guides supporting quasi-periodic variations (Roberts, Edwin, & Benz 1983).

There is increasing evidence to suggest that oscillations in the solar atmosphere can be triggered by flares and other nearby impulsive events. Kane et al. (1983) observed 8 s pulsations of large amplitude during the hard X-ray (HXR) and microwave bursts of a solar flare, while McKenzie & Mullan (1997) have reported periods of 10 – 60 s in the active, non-flaring solar corona. Schrijver, Aschwanden, & Title (2002) have shown that oscillation events observed by the *Transition Region and Coronal Explorer (TRACE)* are often triggered by flares and filament eruptions, occurring in closed coronal loops with no clear dependence of the oscillation amplitude on the magnitude of the flare. Lower in the atmosphere, McAteer et al. (2005) have shown that a flare induced an oscillatory signal along an H α ribbon.

The solar analogy is often used to interpret the wide range of phenomena observed in active stars. Quasi-periodic fluctuations (≈ 30 s) of varying amplitude were reported in the quiescent state of active flare stars and were considered to be a signature of microvariability (Andrews 1989). A similar study by Mullan, Herr, & Bhattacharyya (1992) reported periodicities of a few minutes which were interpreted as transient oscillations in coronal loops. There are also some reports of periodic intensity variations during stellar flares. Short duration variations (10 – 20 s) were reported after the onset of a strong flare on the Hyades star II Tau (Rodonó 1976), while Mathioudakis et al. (2003) reported a large amplitude periodicity (220 s) during the peak of a flare on the RS CVn binary II Peg. The first stellar flare oscillation in X-rays was recently reported by Mitra-Kraev et al. (2005).

Quasi-periodic oscillations during flares can be generated by both the second harmonic of the acoustic mode (Nakariakov et al. 2004, Tsiklauri et al. 2004) and the fundamental mode (Taroyan et al. 2005). The numerical modeling shows that the loop density exhibits perturbations with a maximum near the loop apex, with the oscillation period dependent on the ratio of the loop length to the sound speed (Roberts, Edwin, & Benz 1984). This approach is particularly useful when applied to stellar flares as it provides a method for determining the spatial dimensions of stellar coronal loops.

EQ Peg (Gl 896AB) is a visual binary system with a separation of 5". Both components are M-type flare stars with visual magnitudes of 10.3 and 12.4, respectively. Flare activity on the system has been observed over a large part of the electromagnetic spectrum from X-rays to radio wavelengths. In white light, the flare frequency of the binary is ~ 0.8 flares hr^{-1} for flares with energy in excess of 10^{30} ergs (Lacy, Moffett, & Evans 1976).

Small-amplitude stellar variations are often met with some skepticism as they may be due to sky fluctuations. To bypass this difficulty multi-site observations may be used (Zhilyaev et al. 2000). Here we use high-cadence, multi-wavelength photometry to study periodic intensity variations during a flare on EQ PegB. Synchronous observations of a comparison star were obtained

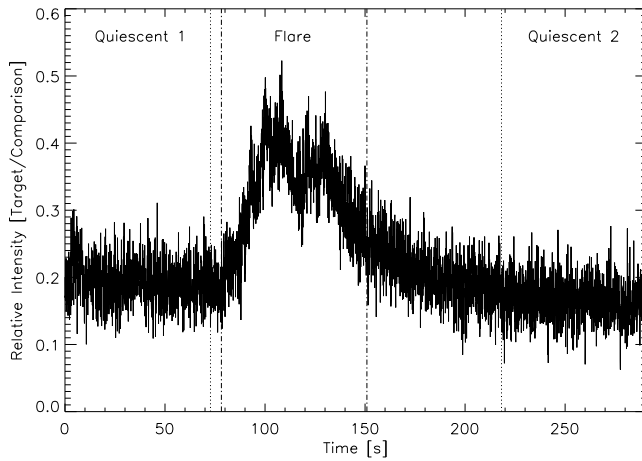


Fig. 1. The u' -band lightcurve of the analyzed flare on EQ PegB. Time is given in seconds since 21:32:53 UT on November 4th 2003.

in order to remove any atmospheric variations. Section 2 details the instrumentation and observations, with the form of time series analysis presented in Section 3. The results are discussed in Section 4, while our conclusions are drawn in Section 5.

2. Observations and data reduction

The observations presented here were obtained with the triple-beam CCD instrument ULTRACAM (Dhillon & Marsh 2001). The instrument uses two dichroic beam-splitters to separate the light into three wavelengths which pass through differing Sloan (SDSS) filters. The detector system comprises of three back-illuminated Marconi 1024x1024 frame-transfer CCDs, allowing the collection of data in the imaging area while data in the masked area is read out. Each chip is triggered by the same GPS synchronized system clock.

We used ULTRACAM on November 4th 2003 with the 4.2 m William Herschel Telescope on La Palma, resulting in a spatial sampling of $0.3'' \text{ pixel}^{-1}$. The large imaging area of the CCDs allows simultaneous observations of the target and a sufficiently bright comparison star. Smaller windows of $21'' \times 21''$ were used around these objects to minimize the dead time between exposures. The observations were made in the u' , g' , and r' Sloan passbands with an exposure time of ~ 0.073 s. The data were reduced with the ULTRACAM pipeline reduction software. The pipeline uses aperture photometry to produce separate lightcurves for each selected object within the field of view (*i.e.*, both the target and the comparison).

3. Time series analysis

The u' -band lightcurve of the flare on EQ PegB is shown in Figure 1, where the duration of the flare is ≈ 160 s. The impulsive phase of the event is followed by intensity variations which were analyzed by both a Fast Fourier Transform and a wavelet transform. Although wavelet analysis is similar to a windowed Fourier analysis, the latter may be considered as an inefficient method for

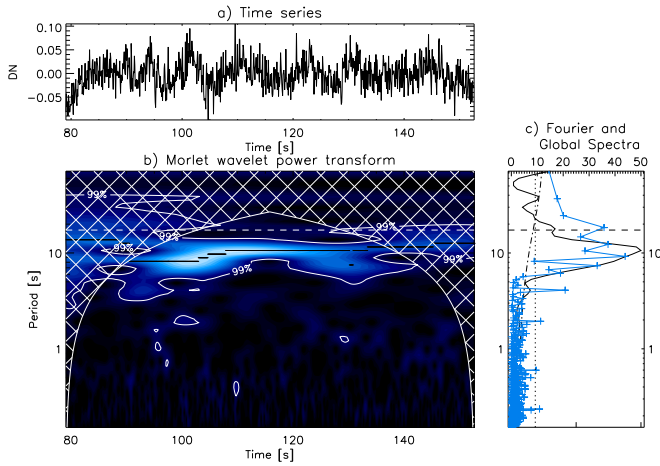


Fig. 2. *a)* The filtered u' -band time series. *b)* The Morlet wavelet power transform of the time series in *a)* as a function of both time (abscissa) and oscillation period (ordinate). Contours define the power above which detections are 99% confident using a two degree of freedom χ^2 distribution. *c)* The global (*i.e.*, averaged) wavelet power (full line) and Fast Fourier power (crosses) as a function of period. The 99% confidence levels are over-plotted for the global wavelet and Fourier curves as dot-dashed and dotted lines, respectively.

the study of quasi-periodic oscillations. This arises not only from Fourier analysis comparing different numbers of oscillatory cycles for differing analysis frequencies, but the windowing process imposes a shorter time interval on the time series within which the analysis is carried out. Hence, the frequency resolution of the Fourier analysis is degraded since $\Delta\nu = 1/T$, where T is the analysis duration.

With wavelet analysis the search for periodic signatures is carried out by a time-localized function which is continuous in both frequency and time (Torrence & Compo 1998), making it well suited for the identification of transient oscillations. Wavelets have become the preferred analysis technique in recent years because wave phenomena in solar and stellar atmospheres have finite durations. An extensive discussion on the effects that various wavelet parameters have upon their results is given in De Moortel, Munday, & Hood (2004).

The wavelet used in this study is the Morlet function, which is defined as the product of a complex exponential (*i.e.*, sine) wave with a Gaussian envelope,

$$\psi_t(s) = \pi^{-1/4} \exp(i\omega t) \exp\left(\frac{-t^2}{2s^2}\right), \quad (1)$$

where t is the time parameter, s is the wavelet scale (related to the Fourier period by $P = 1.03s$ for the Morlet function), ω is the oscillation frequency parameter, and $\pi^{-1/4}$ is a normalization term (Torrence & Compo 1998). By varying the scale of the wavelet function (*i.e.*, both the Gaussian width and the oscillation period) such that the sinusoidal portion matches a given oscillation frequency, the wavelet is convolved with the time series to determine the contribution

of that frequency to the time series. At each wavelet scale, the timing information is achieved by scanning the wavelet function through the time series.

The portions of the u' , g' , and r' time series occurring between the vertical dot–dashed lines in Figure 1 were filtered using wavelet reconstruction to remove the long–period power associated with the general flare profile. This technique rebuilds the time series, x_t , from the wavelet transform, $W_t(s)$, using only information from the desired scale values, s_j ,

$$x_t = \frac{\delta j \delta t^{1/2}}{C_\delta \psi_0(0)} \sum_{j=0}^J \frac{\Re\{W_t(s_j)\}}{s_j^{1/2}}, \quad (2)$$

where δj defines the degree of frequency sampling (taken as 1/32 here), δt is the cadence (0.073 s), and both C_δ and $\psi_0(0)$ are constants (0.776 and $\pi^{-1/4}$ for the Morlet wavelet, respectively). The time series presented here were reconstructed over all scale values corresponding to periods less than 17 s, a point discussed in more detail later. The wavelet power transform of our filtered u' –band time series is shown in Figure 2 where regions of lighter shading indicate greater oscillatory power. The cross–hatched area is the cone of influence (COI) and defines the region of the power spectrum where edge effects may become important due to the finite duration of the time series — the extent of the COI at each period is the e –folding or decorrelation time of the wavelet function.

The reliability of any oscillatory power seen in our data is tested against a number of criteria:

1. Power is tested against spurious detections which could be due to Poisson noise. The contours in Figure 2b outline the power at which detections are 99% confident using a two degree of freedom χ^2 distribution.
2. Time series are compared to a large number of randomized series (1500) with identical count statistics. If there are no periodic signals in the data the measured peak power values should not depend on their observation times. A random–detection probability, p , is calculated for the peak wavelet power at each point in time by comparing the number of times that the random series produce equal or greater power than the actual data — high values indicating no periodic signals in the data while low values suggest the detected peak power periods are real. Confidence levels are calculated from $(1 - p) \times 100$ and are shown for each of our time series in the lower panel of Figure 3.
3. As mentioned previously, the extent of the COI is the decorrelation time of the wavelet function. For the Morlet wavelet this is $\sqrt{2}P$, where P is the oscillatory period. The choice of cutoff period for the filtering (17 s) was based on this value, as longer periods (*i.e.*, those above the dashed line in Figure 2b) can not exist for a decorrelation duration outside the COI. To minimize the chance of detecting noise spikes, we require real detections to have power above the 99% confidence level for at least three oscillatory cycles (*i.e.*, two decorrelation durations).

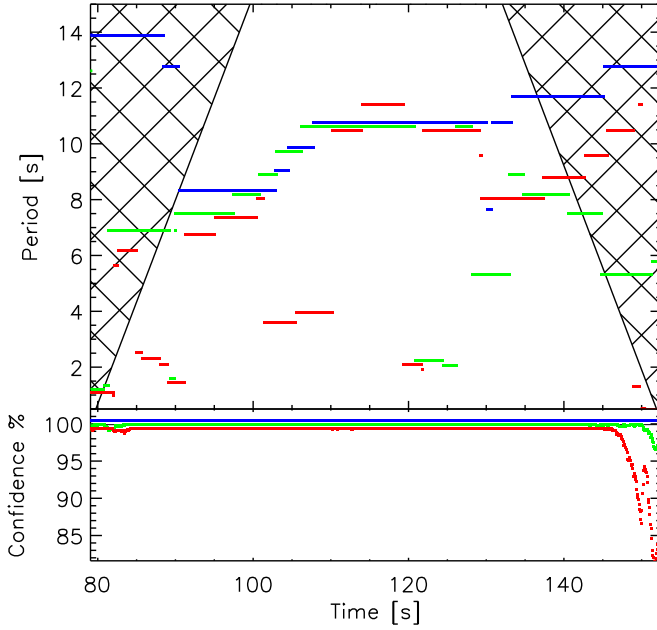


Fig. 3. *Upper:* Oscillation period exhibiting the peak wavelet power at each point in time. *Lower:* Confidence levels achieved by peak wavelet power through randomization testing. In both panels the results from the u' (blue), g' (green), and r' (red) bands are plotted separately.

4. Results and discussion

Our analysis shows a reliable oscillation with a period of ≈ 10 s during the flare on EQ PegB. The oscillation starts just before flare maximum ($t \approx 100$ s) and continues into the decay phase. We conclude that it is due to white-light continuum variations rather than the Balmer and Ca II H&K lines which can provide a significant contribution to the u' -band flux during a flare, because it is seen in all three bands (u' , g' , and r'). The following interpretations may be considered.

4.1. An impulsively-generated acoustic wave

The generation of standing, slow-mode waves in active, coronal loops which are anchored in the photosphere was first proposed by Roberts, Edwin, & Benz (1984). Assuming both a strong longitudinal component (in order to yield density and hence intensity variations) and that the magnetic field dominates sufficiently to approximate the longitudinal tube speed with the acoustic speed, the period of a standing, slow-mode oscillation is given by,

$$P(s) \approx \frac{2L(Mm)}{7.6 \times 10^{-2} N \sqrt{T(MK)}}, \quad (3)$$

where T is the average temperature along the loop, L is the length of the loop, and N is the mode of oscillation (*i.e.*, 1 yields the fundamental mode, 2 the second harmonic). In Figure 3 we show the oscillatory periods exhibiting the maximum power at each point in time. In all three ULTRACAM bands, the period shifts to longer values during the decay phase of the flare. This behaviour can be explained by the standing, acoustic-wave model as a result of a temperature

decrease and/or increase in loop length after the flare peak. Substituting the detected oscillation period (10 s) and a temperature of 20 MK into Equation 3 we obtain a loop length of ≈ 1.7 Mm ($0.0075R_{\star}$) for the fundamental mode and ≈ 3.4 Mm ($0.015R_{\star}$) for the second harmonic.

In a recent numerical model, Nakariakov et al. (2004) have shown that the standing second harmonic of an acoustic wave can be excited in a flaring loop. The excitation of these oscillations is almost independent of the location of the heat deposition in the loop (Tsiklauri et al. 2004) and appears as a natural response of the loop to an impulsive energy deposition. Taroyan et al. (2005) have also examined the excitation of acoustic waves as a result of an impulsive energy deposition at the chromospheric footpoint of a loop. They show that different pulses at the footpoint result in oscillations with the fundamental-mode period. Only pulses with a duration equal to the fundamental-mode period manage to set up standing waves, the rest generate propagating waves.

In these models, the density fluctuations that are generated at the end of the coronal loops, which are located at the top of the chromosphere, may account for the variation of the optical emission (see Fig. 2 in Nakariakov et al. 2004). Alternatively, the optical emission could arise from the free-free emission of coronal loops, as suggested by Mullan et al. (1992). Stepanov et al. (2005) have criticized the latter interpretation as it would imply a high plasma- β which would make the loops unstable. However, since we are considering a flare loop, which is intrinsically unstable, the Mullan et al. (1992) interpretation can not be excluded.

We would like to re-emphasize that one of the main difficulties with the acoustic interpretation is the very small loop length. This implies an extremely large modulation depth due to the flare site occupying a small fraction of the stellar surface. This difficulty has also been pointed out by Stepanov et al. (2005) for a flare on EV Lac.

4.2. A fast-magnetoacoustic wave — the sausage mode

The global sausage mode (GSM) is a fast-MHD mode which can efficiently modulate the plasma density and magnetic field strength. It is also one of the principal modes that can be excited in coronal loops. The modulation of the optical emission from the loop footpoints is determined by the flux of the high-energy electrons which penetrate the lower atmosphere (Stepanov et al. 2005). The sausage mode can be supported if the loops are sufficiently thick and dense. In order to assess whether the GSM can be supported in this flare we require information on the loop length, temperature, density and magnetic field strength. Mullan et al. (2006) have shown that EUV and X-ray observations provide a powerful tool for estimating the physical parameters in the flaring loops of active stars with EQ Peg being one of the stars in their study. For this flare we select a temperature $T = 5 \times 10^7$ K, an internal loop density of $n_e^f = 4 \times 10^{12}$ cm $^{-3}$, a loop length of $L = 1.8 \times 10^9$ cm ($0.14R_{\star}$), and a field strength of $B = 1100$ G (Mullan et al. 2006).

We assume that the quiescent electron density is $n_e^q = 4 \times 10^{11} \text{ cm}^{-3}$. The GSM exists if the dimensionless wave number, $k_c\alpha$, is greater than the cut-off value,

$$k_c\alpha = j_0 \sqrt{\frac{(C_{S0}^2 + C_{A0}^2)(C_{Ae}^2 - C_{T0}^2)}{(C_{Ae}^2 - C_{A0}^2)(C_{Ae}^2 - C_{s0}^2)}} \quad (4)$$

where α is the loop radius and $j_0 = 2.4$. C_{A0} and C_{Ae} are the internal and external Alfvén speeds, while C_{S0} and C_{T0} are the internal sound and tube speeds, respectively. We will follow the criteria outlined in Nakariakov et al. (2003) to determine if this mode can explain the oscillations detected in the EQ PegB flare. Using the loop parameters, we calculate $C_{A0} = 1,200 \text{ km s}^{-1}$, $C_{Ae} = 5,560 \text{ km s}^{-1}$, $C_{s0} = 1,175 \text{ km s}^{-1}$ and $C_{T0} = 840 \text{ km s}^{-1}$. This leads to $k_c\alpha = 0.75$ and $\alpha = 0.24L$. The ratio of the Alfvén speeds is consistent with these parameters ($L/2\alpha < \frac{\pi C_{Ae}}{2j_0 C_{A0}}$). The phase speed $C_p = \frac{2L}{P} = 3,600 \text{ km s}^{-1}$, which is less than the cut-off value ($C_p(k_c) = C_{Ae}$) of the GSM. Finally, the internal Alfvén speed and loop radius estimated above would imply that the period for the GSM should be $P_{GSM} < \frac{2\pi\alpha}{j_0 C_{A0}} = 9.3 \text{ s}$. We conclude that a fast-MHD wave (*i.e.*, the sausage mode) could explain the oscillation detected in this flare, because the shortest period detected is 8 s (Figure 3).

4.3. Individual flare bursts

A detailed survey of solar white-light flares observed with both *TRACE* and the *Reuven Ramaty High Energy Solar Spectroscopic Imager* has confirmed the strong association of white-light emission with HXR emission (Hudson, Wolfson, & Metcalf 2006). Some solar HXR bursts show a high degree of periodicity and have been attributed to the periodic injection of electron beams into the chromosphere (Aschwanden et al. 1994). They suggest that the repetitive injection of beams is governed by a single quasi-periodic accelerator rather than a spatially fragmented system.

The intensity variations observed during the flare on EQ PegB could also be attributed to a group of individual bursts occurring at $\tau \approx 10 \text{ s}$ intervals. Emslie (1981) used an interacting-loop model to explain the time structure and periodicity observed in solar-HXR bursts. In his model, the impulsive energy released in one flare loop creates a disturbance in the surrounding field lines. The disturbance propagates roughly horizontally with a speed approximately equal to the Alfvén speed, $V_A = B/(4\pi n_H m_H)^{1/2}$, until it encounters a neighbouring loop at a spatial separation of $D \approx V_A \tau$. The second loop is triggered and produces a burst which is spatially and temporally different from the first one. Spectroscopic measurements of photospheric magnetic field strengths in active M stars have revealed values in the range 2,000 – 4,000 G (Saar & Linsky 1985, Saar et al. 1986). Adopting a value of 3,000 G for EQ PegB and a hydrogen number density from the stellar atmosphere models of Hawley & Fisher (1992), we derive a sequential loop separation of $D \approx 1 \text{ Mm}$ for the series of loops. The drift to larger τ implies an increase of spatial separation with time during the flare.

5. Concluding remarks

High time resolution, ground-based observations of a white-light flare on an active, fully-convective star reveal intensity variations in continuum emission with a period of ≈ 10 s. The variations are observed in the Sloan u' , g' , and r' bands using synchronous observations of a comparison star to eliminate the possibility that these perturbations are due to changes in the Earth's atmosphere. If the variations are interpreted as an impulsively-excited, standing-longitudinal wave, the period of the oscillation carries information on the physical properties of the medium in which it occurs. However, one of the main drawbacks of the acoustic wave interpretation is that it predicts a very small loop length, which may be unrealistic given the large amount of energy involved during the event. Using typical coronal loop parameters for EQ PegB, we show that a fast-MHD wave, the sausage mode, could provide a more viable interpretation for the observed oscillation. The observations show the potential of applying solar atmospheric seismology techniques to stellar studies.

A series of individual bursts arising from periodic magnetic reconnection could also explain the periodic variations observed. Although reconnection is a dynamic phenomenon with a high degree of intermittency it may lead to periodic signatures. For example, one of the main characteristics of the Tajima et al. (1987) current loop coalescence model is the appearance of quasi-periodic oscillations in the electric and magnetic field energies and ion temperature. The electric field explosively increases and subsequently oscillates as the magnetic flux in the coalesced loops is alternatively compressed and decompressed. A promising interpretation, suggested recently by Nakariakov et al. (2006), involves the MHD oscillation of a non-flaring loop (*i.e.*, the driver) interacting with a flaring active region. This interaction can lead to periodic variations of the current density with a modulation depth significantly higher than the driving oscillation.

Acknowledgements. This work has been supported by the UK Particle Physics and Astronomy Research Council (PPARC). TRM acknowledges the support of a PPARC Senior Research Fellowship. ULTRACAM is supported by PPARC grant PPA/G/S/2002/00092. We would like to thank Prof. D.J. Mullan and Dr. V. Nakariakov for useful discussion. We would also like to thank the referee, Dr. Stepanov, for his comments and suggestions on the paper.

Andrews, A.D., 1989, *A&A*, 214, 220

Aschwanden, M.J., Benz, A.O., Montello, M.L., 1994, *ApJ*, 431, 432

De Moortel, I., Munday, S.A., Hood, A.W., 2004, *Sol. Phys.*, 222, 203

Dhillon, V.S., & Marsh, T.R., 2001, *New Ast.Rev.*, 45, 91

Emslie, A.G., 1981, *Astrophysical Letters*, 22, 41

Hawley, S.L., Fisher, G.H., 1992, *ApJS*, 78, 565

Hudson, H.S., Wolfson, C.J., Metcalf, T.R., 2006, *Sol. Phys.*, in press

Kane, S.R., et al., 1983, *ApJ*, 271, 376

Lacy, C.H., Moffett, T.J., Evans, D.S., 1976, *ApJS*, 30, 85

Mathioudakis, M., et al. 2003, *A&A*, 403, 1101

McAteer, R.T.J., et al. 2005, *ApJ*, 620, 1101

- McKenzie, D.E., & Mullan, D.J. 1997, *Sol. Phys.*, 176, 127
- Mitra-Kraev, U., Harra, L.K., Williams, D.R., Kraev, E. 2005, *A&A*, 436, 1041
- Mullan, D.J., Herr, R.B., Bhattacharyya, S., 1992, *ApJ*, 391, 265
- Mullan, D.J., Mathioudakis, M., Bloomfield, D.S., Christian, D.J. 2006, *ApJS*, in press
- Nakariakov, V.M., Ofman, L., 2001, *A&A*, 327, L53
- Nakariakov, V.M., Melnikov, V.F., Reznikova, V.E., 2003, *A&A*, 412, L7
- Nakariakov, V.M., et al., 2004, *A&A*, 414, L25
- Nakariakov, V. M., Verwichte, E. 2005, *Living Rev. Solar Phys.*, 2, 3
<http://www.livingreviews.org/lrsp-2005-3>
- Nakariakov, V. M., Foullon, C., Verwichte, E., Young, N.P., 2006, *A&A*, in press
- Roberts, B., Edwin, P.M., Benz, A.O., 1983, *Nature*, 305, 688
- Roberts, B., Edwin, P.M., Benz, A.O., 1984, *ApJ*, 279, 857
- Roberts, B. 2000, *Sol. Phys.*, 193, 139
- Rodonó, M., 1976, *A&A*, 32, 337
- Saar, S.H., Linsky, J.L., 1985, *ApJ*, 299, L47
- Saar, S.H., Linsky, J.L., Beckers, J.M., 1986, *A&A*, 302, 777
- Schrijver, C.J., Aschwanden, M.J., Title, A.M., 2002, *Sol. Phys.*, 206, 69
- Stepanov, A.V., Kopylova, Y.G., Tsap, Y.T., Kupriyanova, E.G., 2005, *Astron. Lett.* 31, 612
- Tajima, T., et al., 1987, *ApJ*, 321, 1031
- Taroyan, Y., Erdélyi, R., Doyle, J.G., Bradshaw, S.J., 2005, *A&A*, 438, 713
- Torrence, C., Compo, G.P., 1998, *Bull. Am. Meteor. Soc.* 79, 61
- Tsiklauri, D., Aschwanden, M.J., Nakariakov, V.M., Arber, T.D., 2004, *A&A*, 419, 1149
- Zhilyaev et al. 2000, *A&A*, 364, 641